J Mater Sci (2011) 46:3216–3224
DOI 10.1007/s10853-010-5206-9

Effects of minor Zr and Sr on as-cast microstructure and mechanical properties of Mg–3Ce–1.2Mn–1Zn (wt%) magnesium alloy

Mingbo Yang · Fusheng Pan · Xiaofeng Liang · Jia Shen · Caiyuan Qin

Received: 5 October 2010 / Accepted: 17 December 2010 / Published online: 29 December 2010

Abstract The effects of minor Zr and Sr on the as-cast microstructure and mechanical properties of the Mg–3Ce–1.2Mn–1Zn (wt%) alloy were investigated. The results indicate that adding minor Zr and/or Sr to the Mg–3Ce–1.2Mn–1Zn alloy does not cause an obvious change in the morphology and distribution of the $Mg_{12}Ce$ phase. However, the grains of the Zr- and/or Sr-containing alloys are effectively refined. Among the Zr- and/or Sr-containing alloys, the grains of the alloy with the addition of 0.5 wt%Zr + 0.1 wt%Sr are the finest. Furthermore, adding minor Zr and/or Sr to the Mg–3Ce–1.2Mn–1Zn alloy can improve the tensile properties. Among the Zr- and/or Sr-containing alloys, the alloy with the addition of 0.5 wt%Zr + 0.1 wt%Sr obtains the optimum tensile properties. In addition, adding minor Zr and/or Sr to the Mg–3Ce–1.2Mn–1Zn alloy also can improve the creep properties, and the creep properties of the three alloys with the additions of 0.5 wt%Zr + 0.1 wt%Sr, 0.5 wt%Zr, and 0.1 wt%Sr are similar.

M. Yang (✉) · X. Liang · J. Shen · C. Qin
Materials Science & Engineering College, Chongqing University of Technology, Chongqing 400054, China
e-mail: yangmingbo@cqut.edu.cn

M. Yang · F. Pan
National Engineering Research Center for Magnesium Alloys, Chongqing University, Chongqing 400030, China

M. Yang
Key Laboratory of Automobile Components Manufacturing and Testing Technology of the Education Ministry, Chongqing University of Technology, Chongqing 400054, China

Introduction

At present, the development of new magnesium alloys is becoming increasingly important due to the potential saving in weight when compared to aluminum-based alloys. However, the creep properties of magnesium alloys are limited by their low melting point which can vary depending on the alloying content [1]. Hence, the development of elevated temperature magnesium alloys is necessary to compete with other light constructional materials such as aluminum alloys and improve the temperature range of application of magnesium components. Previous investigations indicated that magnesium alloys based on the Mg–Sc system exhibited interesting properties [2, 3], and it was further found that the additions of Mn and Ce to Mg–Sc alloys could improve the creep resistance substantially [4, 5]. For example, the quaternary Mg–Ce–Mn–Sc alloys are considerably superior to WE alloys and exhibit high creep resistance at high temperatures over 300 °C [5, 6]. However, due to the expensive scandium, the application of the Mg–Ce–Mn–Sc alloys is limited. Therefore, the research of replacing expensive scandium by cheap alloying elements for the Mg–Ce–Mn–Sc alloys needs to be considered. Since Zn can form intermetallic phases with Mg and/or RE as plates on basal planes of α-Mg matrix and Smola et al. [7] found that the Mg–4Y–1Mn–1Zn alloy exhibited higher creep properties than the Mg–4Y–1Mn–1Sc alloy, it is expected that Zn is the possible less expensive alternative to Sc in the Mg–Ce–Mn–Sc alloys and then some research on the Mg–Ce–Mn-Zn alloys has been carried out. Recent investigations indicated that the Mg–Ce–Mn–Zn alloys have similar mechanical properties at room temperature and 300 °C as compared with the Mg–Ce–Mn–Sc alloys [7, 8]. However, it is further reported that, similar to the quaternary Mg–Ce–Mn–Sc

alloys, the grains of the quaternary Mg–Ce–Mn–Zn alloys also are relatively coarse, leading to the relatively poor mechanical properties [8]. Therefore, further enhancement in the mechanical properties for the quaternary Mg–Ce–Mn–Zn alloys by grain refinement needs to be considered.

It is well known that Zr is a powerful grain refiner for Mg-RE alloys to further improve the mechanical properties, and the Zr-containing magnesium alloys usually show a higher corrosion resistance than the Zr-free magnesium alloys [9]. In addition, it is also known that the Sr addition can refine the microstructures, improve the strength and creep resistance of magnesium alloys [10, 11], and Zhao et al. [12] found that adding minor Sr to the Mg–3.5Mn alloy could refine the grains of the alloy and thus lead to the improvement of the tensile strength and toughness. Although Emley et al. [13, 14] reported that Zr could not be used in the Mn-containing magnesium alloys, the powerful evidence is not provided and some Mn- and Zr-containing magnesium alloys such as Mg–Y–Mn–Zr alloys are being developed [15, 16]. Therefore, it is expected that the Zr and/or Sr additions to the Mg–Ce–Mn–Zn alloy are possibly beneficial to the microstructural refinement and the improvement of mechanical properties. Due to the above-mentioned reasons, this study investigates the effects of minor Zr and/or Sr on the as-cast microstructure and mechanical properties of the Mg–3Ce–1.2Mn–1Zn magnesium alloy.

Experimental procedures

The nominal compositions (wt%) of the experimental alloys studied in this work are Mg–3Ce–1.2Mn–1Zn ($1^{\#}$ alloy), Mg–3Ce–1.2Mn–1Zn–0.5Zr ($2^{\#}$ alloy), Mg–3Ce–1.2Mn–1Zn–0.1Sr ($3^{\#}$ alloy), and Mg–3Ce–1.2Mn–1Zn–0.5Zr–0.1Sr ($4^{\#}$ alloy). The experimental alloys were prepared by adding pure Mg and Zn, Mg–29.24 wt%Ce, Mg–4.38 wt%Mn, Mg–31.27 wt%Zr, and Mg–10 wt%Sr master alloys. The experimental alloys were melted in a crucible resistance furnace and protected by a flux addition. After being held at 740 °C for 20 min, the melts of the experimental alloys were, respectively, homogenized by mechanical stirring and then poured into a permanent mold which was coated and preheated to 200 °C to obtain a casting. The specimens as shown in Fig. 1 were fabricated from the castings for tensile and creep tests. Furthermore, the samples of the experimental alloys were subjected to a solution heat treatment (520 °C/12 h + water cooled) to reveal the grain boundaries and examine the microstructural stability at high temperatures. Table 1 lists the actual chemical compositions of the experimental alloys, which were inspected by inductively coupled plasma spectroscopy.

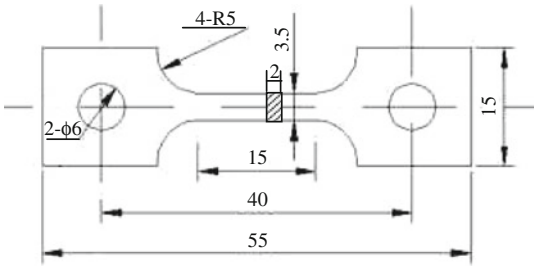

Fig. 1 Configuration of the samples used for the tensile and creep tests (unit: mm)

Table 1 Actual compositions of the experimental alloys, wt%

Experimental alloys	Ce	Mn	Zn	Zr	Sr	Mg
$1^{\#}$ (Mg–3Ce–1.2Mn–1Zn)	2.76	1.08	0.92	–	–	Bal.
$2^{\#}$ (Mg–3Ce–1.2Mn–1Zn–0.5Zr)	2.80	1.05	0.90	0.38	–	Bal.
$3^{\#}$ (Mg–3Ce–1.2Mn–1Zn–0.1Sr)	2.77	1.08	0.93	–	0.08	Bal.
$4^{\#}$ (Mg–3Ce–1.2Mn–1Zn–0.5Zr–0.1Sr)	2.79	1.11	0.92	0.40	0.07	Bal.

In order to analyze the solidification behavior of the experimental alloys, the differential scanning calorimetry (DSC) was carried out using a NETZSCH STA 449C system equipped with platinum–rhodium crucibles. Samples weighing around 30 mg were heated in a flowing argon atmosphere from 30 to 700 °C for 5 min before being cooled down to 100 °C. The heating and cooling curves were recorded at a controlling speed of 15 °C/min.

The as-cast and solutionized samples of the experimental alloys were, respectively, etched in an 8% nitric acid solution in distilled water and a solution of 1.5 g picric, 25 mL ethanol, 5 mL acetic acid, and 10 mL distilled water, and then were examined by an Olympus optical microscope and/or JEOL JSM-6460LV type scanning electron microscope equipped with Oxford energy dispersive X-ray spectrometer (EDS) with an operating voltage of 20 kV. The phases in the as-cast experimental alloys were also analyzed by D/Max-1200X type analyzer operated at 40 kV and 30 mA. The grain size was analyzed by the standard linear intercept method using an Olympus stereomicroscope. The as-cast tensile properties of the experimental alloys at room temperature and 300 °C were determined from a complete stress–strain curve. Ultimate tensile strength (UTS), 0.2% yield strength (YS), and elongation to failure (Elong.) were obtained based on the average value of three tests. Constant-load tensile creep tests were performed at 300 °C and 30 MPa for creep extension up to 100 h. The minimum creep rates of the as-cast experimental alloys were measured from each elongation-time curve and averaged over three tests.

Results and discussion

Effects on as-cast microstructure

Figure 2 shows the XRD results of the as-cast experimental alloys. As shown in Fig. 2, all the experimental alloys are mainly composed of α-Mg and $Mg_{12}Ce$ phases, and no Zn-containing phases are identified in the alloy. In addition, the Mn_2Zr phase which has been reported in the Mg–4Y–1Mn–1Zr alloy [15] is not observed in the XRD results of the Zr-containing experimental alloys, which is possibly related to the low content of Zr in the experimental alloys. Actually, the XRD results may be further confirmed by the DSC results of the as-cast alloys. Figure 3 shows the DSC cooling curves of the as-cast alloys. It is found from Fig. 3 that the DSC cooling curves of the experimental alloys are similar, with two main peaks in the cooling curves, indicating that adding minor Zr and/or Sr to the Mg–3Ce–1.2Mn–1Zn alloy does not influence the types of the phase transformations of the alloy. Based on the DSC results, it is preliminarily inferred that during the solidification of the experimental alloys the primary α-Mg phase first nucleates and grows until the temperature falls to about 580 °C where a binary eutectic reaction ($L_1 \rightarrow$ α-Mg + $Mg_{12}Ce$) occurs. Accordingly, the final microstructure of the experimental alloys mainly consists of α-Mg and $Mg_{12}Ce$ phases.

Figure 4 shows the optical images of the as-cast experimental alloys. It is observed from Fig. 4 that the primary α-Mg phases in the as-cast experimental alloys mainly display a dendrite configuration. Furthermore, it is found from Fig. 4 that the dendrite arm spacings of the primary α-Mg phases in the Zr- and/or Sr-containing alloys are relatively smaller than those in the quaternary alloy, indicating that adding minor Zr and/or Sr to the Mg–3Ce–1.2Mn–1Zn alloy possibly refine the microstructure of the alloy. This is further confirmed from Fig. 5, which shows the optical images of the solutionized experimental alloys. It is observed from Fig. 5 that the Zr- and/or Sr-containing alloys exhibit relatively finer grains than the quaternary alloy. The average grain size before refining is 196 μm (the standard error: 15 μm) for the quaternary alloy and after adding Zr and/or Sr its average size is 87 μm (the standard error: 8 μm), 128 μm (the standard error: 19 μm) and 61 μm (the standard error: 12 μm) for the alloys with 0.5 wt%Zr, 0.1 wt%Sr, and 0.5 wt%Zr + 0.1 wt%Sr, respectively. Obviously, the above results indicate that adding 0.5 wt%Zr + 0.1 wt%Sr to the Mg–3Ce–1.2Mn–1Zn alloy can obtain the highest grain refining efficiency, followed by adding 0.5 wt%Zr and 0.1 wt%Sr, respectively. Since the mechanisms for the grain refinement of the Zr- or Sr-containing magnesium alloys have been described in detail in [17], the following discussions mainly focus on the difference in the grain refinement of the Mg–3Ce–1.2Mn–1Zn alloys with minor Zr and/or Sr. Previous investigations showed that the mechanism for the grain refinement by Zr in the low Zr magnesium alloys is different from that in the high Zr magnesium alloys [17–19]: the grain refinement by a high Zr content (above the peritectic point, 0.59%) commonly relates to the lattice disregistry between Zr and Mg and the grain refinement by a low Zr content (below the peritectic point, 0.59%) is mostly caused by the growth restriction effects of Zr solute during solidification. In addition, the mechanism for the grain refinement by minor Sr in the magnesium alloys is also thought to be related to the growth restriction effects of Sr solute during solidification due to the low solid solubility of Sr in magnesium (about 0.11pct) and the rapid enrichment of solute in the liquid ahead of the growing interface [17]. According to the growth restriction factor (GRF) values for various alloying elements in magnesium alloys [20], Zr has the very high growth restriction factor value (38.29), whereas the growth restriction factor value of Sr is relatively low (3.51). Therefore, the Zr-containing Mg–3Ce–1.2Mn–1Zn alloy obtains a higher grain refinement efficiency than the Sr-containing alloy. As for the highest grain refining efficiency of the Zr- and Sr-containing Mg–3Ce–1.2Mn–1Zn alloy, it is possibly related to the combined effects of Zr and Sr on the growth restriction during solidification. However, this needs further confirmation.

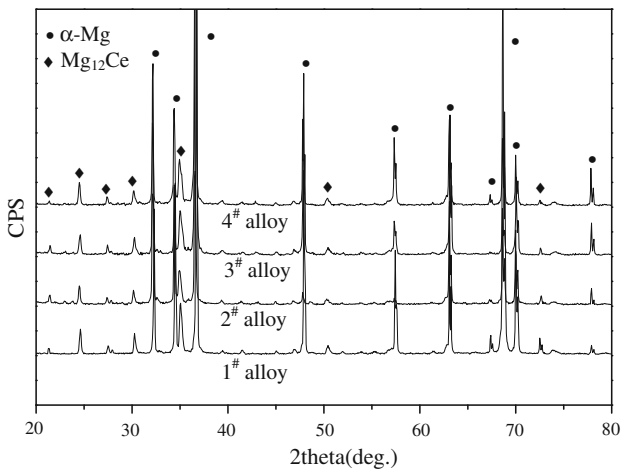

Fig. 2 XRD results of the as-cast alloys

Figure 6 shows the SEM images of the as-cast experimental alloys. In Fig. 6, the second phases are identified by combining the XRD results with the EDS analysis. As shown in Fig. 6, the $Mg_{12}Ce$ phases in the experimental alloys mainly exhibit continuous and/or quasi-continuous nets, and distribute at the grain boundary. Furthermore, a small quantity of the $Mg_{12}Ce$ phases with particle-like shapes are also observed (Fig. 6b, f). Obviously, the

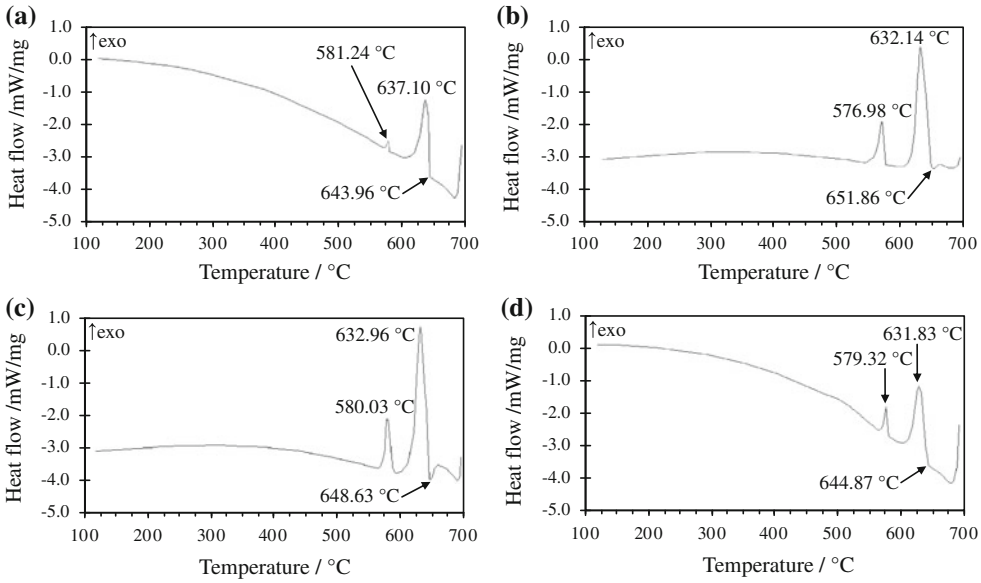

Fig. 3 DSC cooling curves of the as-cast alloys: **a** 1# alloy; **b** 2# alloy; **c** 3# alloy; **d** 4# alloy

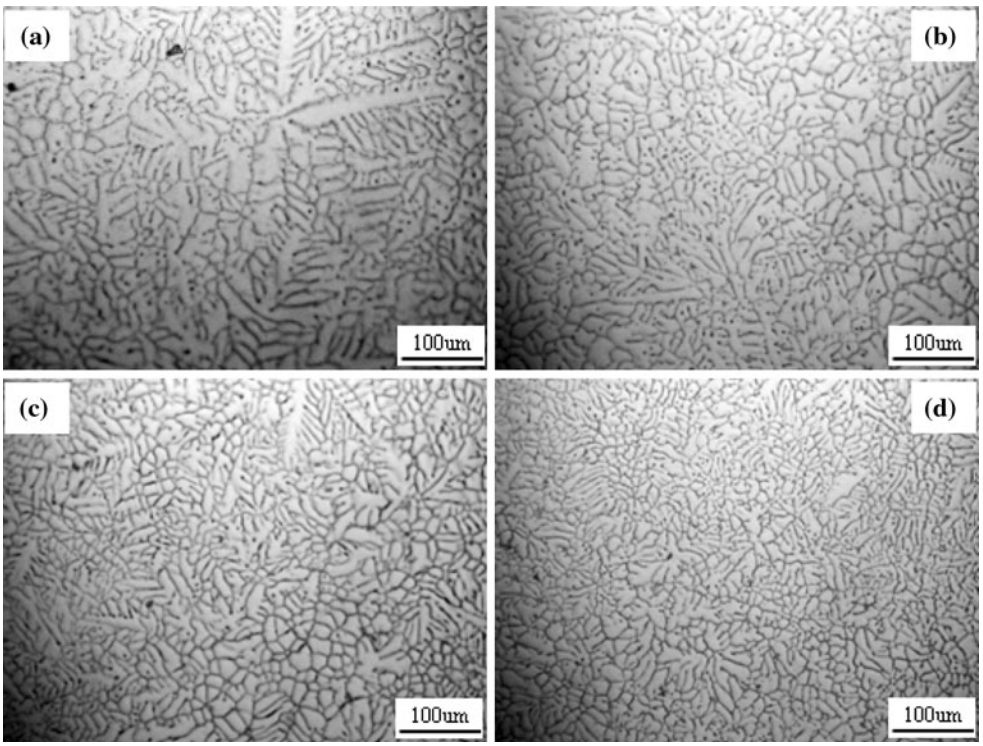

Fig. 4 Optical images of the as-cast alloys: **a** 1# alloy; **b** 2# alloy; **c** 3# alloy; **d** 4# alloy

morphology and distribution of the $Mg_{12}Ce$ phase in the Mg–3Ce–1.2Mn–1Zn alloy are not significantly influenced by the minor Zr and/or Sr additions.

Effects on mechanical properties

The tensile properties, including ultimate tensile strength (UTS), 0.2% yield strength (YS), elongation (Elong.), and creep properties of the as-cast experimental alloys are listed in Table 2. It is observed from Table 2 that the Zr- and/or Sr-containing alloys exhibit relatively higher tensile properties at the room temperature and 300 °C than the quaternary alloy, indicating that adding minor Zr and/or Sr to the Mg–3Ce–1.2Mn–1Zn alloy is beneficial to the improvement of the tensile properties. Furthermore, it is found from Table 2 that among the Zr- and/or Sr-containing alloys the tensile properties of the alloy with 0.5 wt%Zr + 0.1 wt%Sr are highest at the room

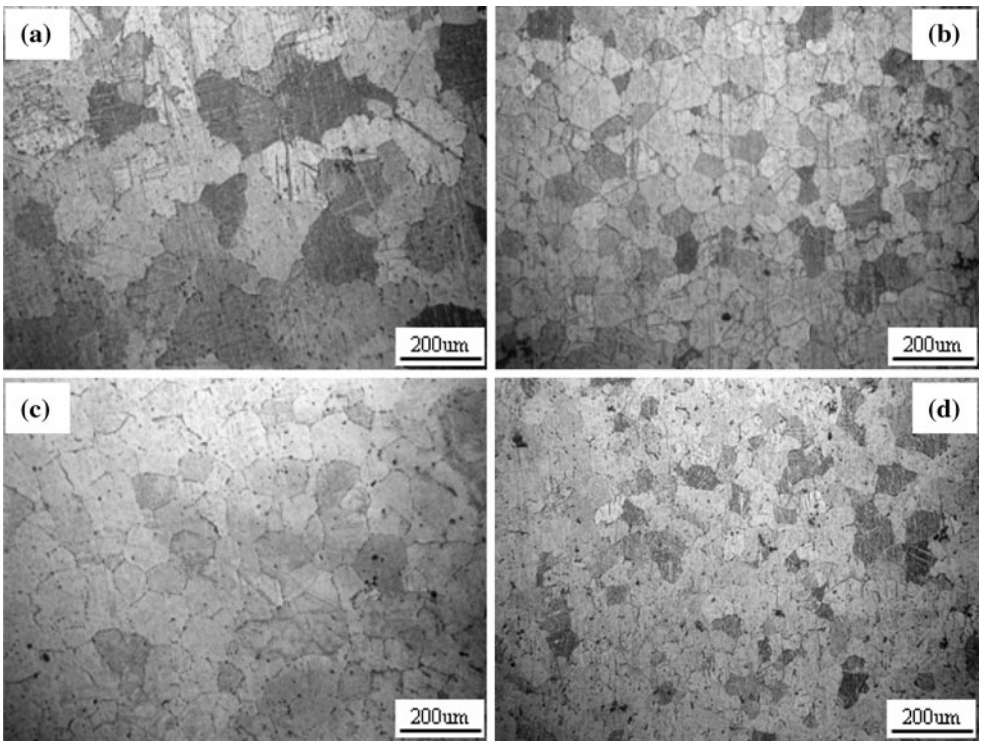

Fig. 5 Optical images of the solutionized alloys: **a** 1# alloy; **b**2# alloy; **c** 3# alloy; **d** 4# alloy

temperature and 300 °C, and followed by the alloys with 0.5 wt%Zr and 0.1 wt%Sr, respectively. Obviously, it can be easily explained by the grain refinement that adding minor Zr and/or Sr to the Mg–3Ce–1.2Mn–1Zn alloy improve the tensile properties of the alloy. Similarly, the highest tensile properties for the Mg–3Ce–1.2Mn–1Zn alloy with 0.5 wt%Zr + 0.1 wt%Sr are also consistent with the smallest grain size of the alloy. The effects of Zr and Sr additions on the tensile properties of the Mg–3Ce–1.2Mn–1Zn alloy can be further confirmed from Figs. 7 and 8. Figures 7 and 8 show the SEM images of tensile fractographs and optical images of longitudinal sections for the as-cast alloys failed in the tensile tests at room temperature, respectively. As shown in Fig. 7, a number of cleavage planes and steps are present, and some river patterns can also be observed in the tensile fracture surfaces of the experimental alloys, indicating that all the tensile fracture surfaces have mixed characteristics of cleavage and quasi-cleavage fractures. Furthermore, it is observed from Fig. 8 that the tensile rupture of the experimental alloys occurs along inter-granular boundary. Obviously, adding minor Zr and/or Sr to the Mg–3Ce–1.2Mn–1Zn alloy does not significantly change the fracture mode of the alloy. However, some very obvious lacerated ridges are observed in the tensile fracture surface of the alloy without adding Zr and Sr, which is consistent with the relatively poor tensile properties of the alloy.

In addition, it is observed from Table 2 that the creep properties of the Zr- and/or Sr-containing alloys are higher than those of the quaternary alloy, indicating minor Zr and/or Sr to the Mg–3Ce–1.2Mn–1Zn alloy can improve the creep properties of the alloy. It is well known that the dispersion strengthening is one major strengthening mechanism for creep resistance of alloys [21]. The second-phase particles can contribute to the creep resistance by obstructing dislocation annihilation in dislocation creep or inhibiting grain boundary migration and/or grain boundary sliding in diffusional creep. Because the difference in the morphology, size, and distribution of the second particles between the alloys, with and without addition of Zr and/or Sr, is small (Fig. 6), the dispersion strengthening cannot explain the difference in the creep properties of the experimental alloys. In addition, it is generally accepted that the rate of dislocation creep tends to decrease with increasing grain size due to a lowered contribution of grain boundary sliding [21]. Since the grain size of the Zr- and/or Sr-containing alloys is smaller than that of the quaternary alloy, the grain size effect cannot explain the difference in the creep properties of the experimental alloys. Obviously, the difference in the creep properties is possibly related to another mechanism. Figure 9 shows the SEM image of the solutionized experimental alloys. It is observed from Fig. 9 that a majority of the $Mg_{12}Ce$ phases in the experimental alloys have dissolved into the matrix after solid solution

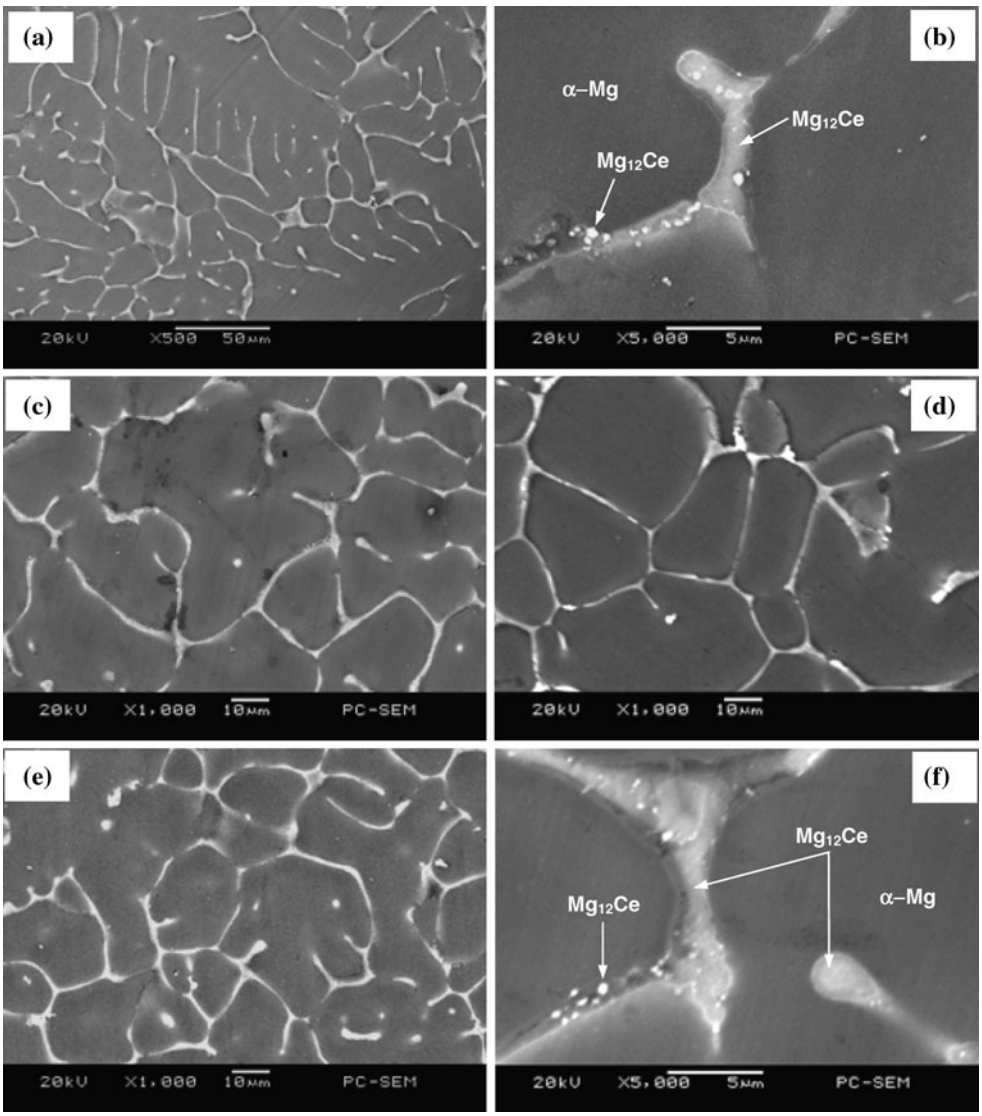

Fig. 6 SEM images of the as-cast alloys: **a**, **b** 1# alloy; **c** 2# alloy; **d** 3# alloy; **e**, **f** 4# alloy

Table 2 Tensile and creep properties of the as-cast alloys

Experimental alloys	Tensile properties						Creep properties	
	Room temperature			300 °C			300 °C and 30 MPa for 100 h	
	UTS (MPa)	YS (MPa)	Elong. (%)	UTS (MPa)	YS (MPa)	Elong. (%)	Total creep strain (%)	Minimum creep rate ($\times 10^{-8}$ s^{-1})
1# alloy	152 (2.8)	130 (2.7)	3.0 (0.19)	101 (2.2)	87 (2.7)	15.6 (1.02)	1.85 (0.08)	5.14 (0.41)
2# alloy	173 (1.9)	141 (2.0)	3.7 (0.15)	130 (3.2)	98 (2.1)	16.8 (1.03)	1.15 (0.05)	3.19 (0.38)
3# alloy	161 (1.7)	136 (2.2)	3.2 (0.12)	122 (2.6)	94 (1.8)	15.9 (1.12)	1.23 (0.08)	3.41 (0.42)
4# alloy	187 (2.2)	149 (1.6)	4.1 (0.14)	137 (2.8)	113 (2.2)	17.9 (1.07)	1.16 (0.06)	3.22 (0.29)

Note: The data in the bracket is the standard error

heat treatment at 520 °C for 12 h. However, it is found that the remnant $Mg_{12}Ce$ phases in the Zr- and/or Sr-containing alloys seem to be more than those in the quaternary alloy. That is, the amount of the remnant $Mg_{12}Ce$ phases in the Zr- and/or Sr-containing alloys seems to be larger, indicating that adding minor Zr and/or Sr to the Mg–3Ce–1.2Mn–1Zn alloy is beneficial to the stability of eutectic $Mg_{12}Ce$ phase at high temperatures. Since the creep

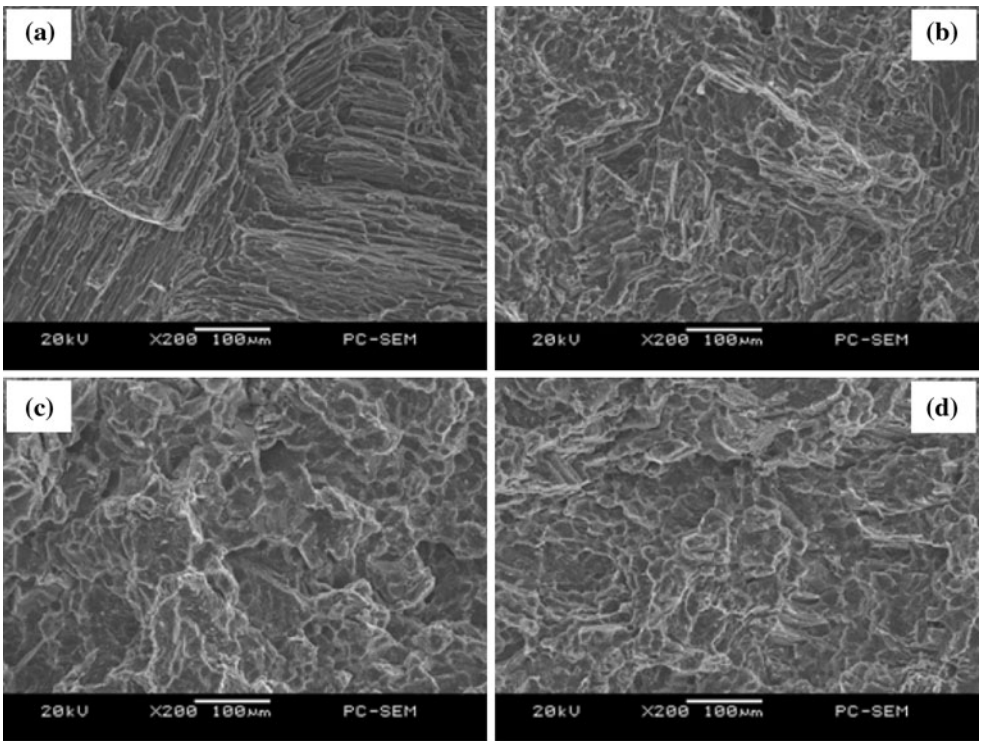

Fig. 7 SEM images of the tensile fractographs for the as-cast alloys tested at room temperature: **a** 1# alloy; **b** 2# alloy; **c** 3# alloy; **d** 4# alloy

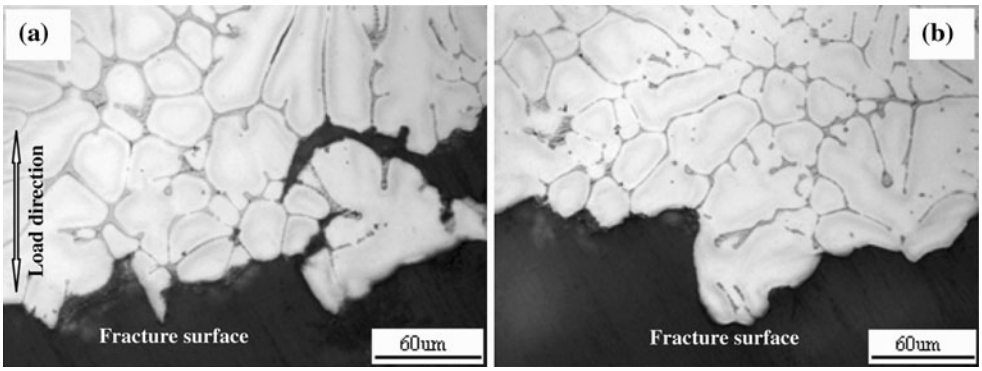

Fig. 8 Optical images of longitudinal sections for the as-cast alloys failed in tensile test at room temperature: **a** 1# alloy; **b** 4# alloy

resistance properties of magnesium alloys are mainly related to the structure stability at high temperatures, it is preliminarily inferred that the improvement of the creep properties for the Zr- and/or Sr-containing Mg–3Ce–1.2Mn–1Zn alloys is possibly related to the effects of Zr and/or Sr additions on the stability of eutectic $Mg_{12}Ce$ phases at high temperatures. However, this needs to be further confirmed. In addition, it is found the microstructural characteristic of the Zr- and/or Sr-containing solutionized alloys is similar, which is consistent with the close creep properties of the three alloy, as listed in Table 2.

Conclusions

(1) Adding minor Zr and/or Sr to the Mg–3Ce–1.2Mn–1Zn alloy does not cause an obvious change in the morphology and distribution of the $Mg_{12}Ce$ phase. However, the grains of the Zr- and/or Sr-containing alloys are effectively refined. Among the Zr- and/or Sr-containing alloys, the grains of the alloy with the addition of 0.5 wt%Zr + 0.1 wt%Sr are the finest, followed by the alloys with the additions of 0.5 wt%Zr and 0.1 wt%Sr, respectively.

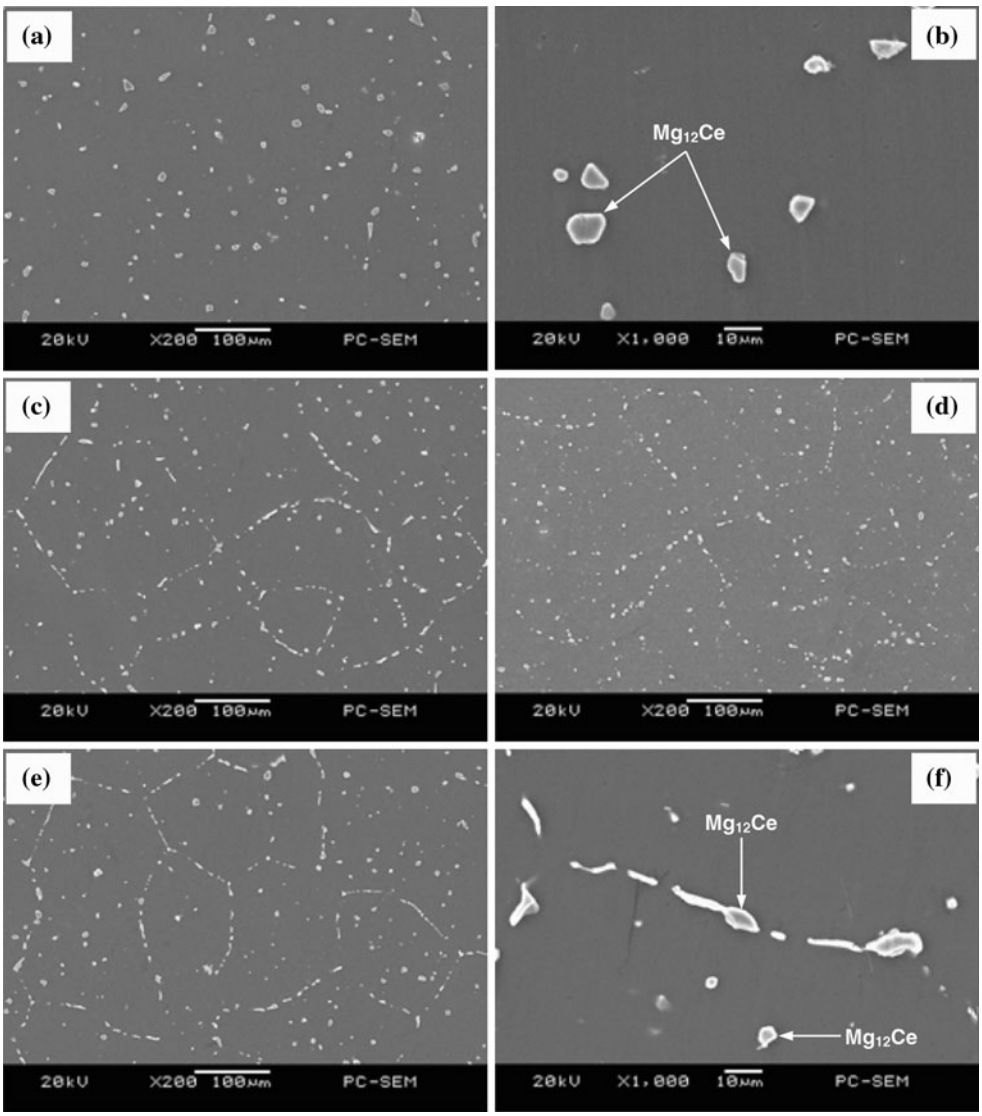

Fig. 9 SEM images of the solutionized alloys: **a**, **b** 1# alloy; **c** 2# alloy; **d** 3# alloy; **e**, **f** 4# alloy

(2) Adding minor Zr and/or Sr to the Mg–3Ce–1.2Mn–1Zn alloy can improve the tensile properties at room temperature and 300 °C. Among the Zr- and/or Sr-containing alloys, the alloy with the addition of 0.5 wt%Zr + 0.1 wt%Sr obtains the optimum tensile properties, followed by the alloys with the additions of 0.5 wt%Zr and 0.1 wt%Sr, respectively. In addition, adding minor Zr and/or Sr to the Mg–3Ce–1.2Mn–1Zn alloy also can improve the creep properties at 300 °C and 30 MPa for 100 h, and the creep properties of the three alloys with the additions of 0.5 wt%Zr + 0.1 wt%Sr, 0.5 wt%Zr, and 0.5 wt%Zr are similar.

Acknowledgements This study was supported by the National Natural Science Funds of China (No. 50725413), the Major State Basic Research Development Program of China (973)(No. 2007CB613704), the Chongqing Science and Technology Commission in China (CSTC, 2010AC4085 and 2009AB4134), and the Program for Hundreds of Distinguished Leading Scientists of CQ CSTC (2010CSTC-HDLS).

References

1. Luo A, Pekguleryuz MZ (1994) J Mater Sci 29:5259. doi: 10.1007/BF01171534
2. Mordike BL, Stulikova I, Smola B (2005) Metal Mater Trans A 36:1729
3. Buch FV, Lietzau J, Mordike BL, Pisch A, Schmid-Fetzer R (1999) Mater Sci Eng A 263:1
4. Mordike BL (2001) J Mater Proc Technol 117:391
5. Stulíkova I, Smola B, Buch FV, Mordike BL (2003) Materialwissenschaft Werkst 34:102
6. Smola B, Stulikova I, Pelcova J, Mordike BI (2004) J Alloy Compd 378:196

7. Smola B, Stulikova I, Pelcova J, Zaludova N (2007) Phase composition and creep behavior of Mg-RE-Mn alloys with Zn addition. In: Kainer KU (eds) Proceedings of 7th international conference on magnesium alloys and their applications, Dresden, Germany, pp 67–72
8. Shen J, Yang MB, Pan FS, Cheng RJ (2009) Mater Sci Forum 610–613:746
9. Ben-Hamu G, Eliezer D, Shin KS, Cohen S (2007) J Alloy Compd 431:269
10. Yang M, Pan F, Cheng R, Tang A (2008) Mater Sci Eng A 491:440
11. Dargusch MS, Zhu SM, Nie JF, Dunlop GL (2009) Scripta Mater 60:116
12. Zhao HF, Wang L, Sun L, Zhang SA, Yan K, Li QF, Liu MY (2009) Mater Res Appl 3:262
13. Emley EF (1966) Principles of magnesium technology. Pergamon, Oxford, p 127
14. Bamberger M, Dehm G (2008) Ann Rev Mater Res 38:505
15. Grobner J, Schmid-Fetzer R (2001) J Alloy Compd 320:296
16. Mordike BL (2002) Mater Sci Eng A 324:103
17. Lee YC, Dahle AK, Stjohn DH (2000) Metal Mater Trans A 31:2895
18. Sun M, Wu GH, Wang W, Ding WJ (2009) Mater Sci Eng A 523:145
19. Peng ZK, Zhang XM, Chen JM, Xiao Y, Jiang H (2005) Mater Sci Technol 21:722
20. Stjohn DH, Qian M, Easton MA, Cao P, Hildebrand Z (2005) Metal Mater Trans A 36:1669
21. Zhu SM, Mordike BL, Nie JF (2008) Mater Sci Eng A 483–484:583